

RELATIONSHIPS BETWEEN VEGETATION INDICES AND RAINFALL AND PET AT DIFFERENT TIME-LAGS: A STUDY AT A MEDITERRANEAN TO ARID GRADIENT

S. Mozhaeva^{1*}, M. Shoshany¹

¹ IIT, Israel Institute of Technology, Civil & Environmental Engineering Faculty, Mapping & Geoinformation Engineering Division, 32000 Haifa, Israel - (sofiam@campus.technion.ac.il, maximsh@technion.ac.il)

Commission III, WG III/10

KEY WORDS: Vegetation Response, NDVI, Rainfall, Potential Evapotranspiration, Climatic Gradient, Regression Analysis, Time-Lag Analysis, Classification.

ABSTRACT:

The climatic gradient between the Judean Lowland and the Negev Desert in Central Israel represents a transition zone between dense shrublands in the North, and desert fringe Batha and Irano-Turanian vegetation in the South, characterizing wide Mediterranean Type Climate regions around the world. Understanding the expected response of these water-limited ecosystems to climate change presents a significant challenge due to the high geodiversity of Mediterranean environments. Studying relationships between vegetation patterns and climatic parameters is fundamental for this purpose, and remote sensing provides a valuable tool for investigating these relationships over large regions. This study aims at examining the relationships between NDVI extracted from Sentinel2 and rainfall and PET accumulated over 1 to 6 months. The analysis was first conducted for 38 sites (100x100 meters) across the climatic gradient for three years representing high (2016), low (2017), and average (2018) rainfall. Results indicate that the highest correlation between NDVI and climatic parameters is achieved for accumulation interval of two months. Least-squares analysis was then utilized for calculating the per-pixel regression coefficients between NDVI and corresponding rainfall and PET. Classification of the multi-temporal NDVI (2016-2018) and of the linear regressions' coefficients between NDVI and rainfall and PET at accumulation interval of 2 months yielded both high accuracies. Since these slope and intercept coefficients can be perceived as representing the water-use regime at each pixel, the similarity between the classification results suggests that multi-temporal NDVI typologies correspond water-use regime typologies across desert fringe ecosystems at the margins of Mediterranean regions.

1. INTRODUCTION

The climatic gradient between the Judean Lowland and the Negev Desert (Figure 1a) represents a transition zone between dense Mediterranean shrublands, open shrublands, desert fringe Batha, and arid ecosystems, which characterize wide desert margins in North Africa, the southern and eastern Mediterranean Basin, western Australia and south Africa, Chile and California. Understanding the expected response of these water-limited ecosystems to climate change presents a significant and important challenge (e.g., Malhi et al., 2020; Gouveia et al., 2017; Gordo and Sanz, 2010). Studying relationships between vegetation patterns and rainfall and PET is fundamental for this purpose, and remote sensing using spectral vegetation indices is instrumental for investigating these relationships over large regions. Examination of NDVI and rainfall relationships appears to be the main approach, implemented over desert and semi-arid regions (Nicholson et al., 1990; Nicholson and Farrar, 1994; Al-Bakri and Suleman, 2004; Chamaille-Jammes et al., 2006; Chamaille-Jammes and Fritz, 2009; Shoshany and Karnibad, 2011;2015; Dagnachew et al., 2020). The inclusion of potential evapotranspiration was reported in a most limited number of previous studies (Dorman et al., 2013; Vicente-Serrano et al., 2013; Islam and Mamun, 2015; Munson et al., 2016; Gouveia et al., 2017; Lamchin et al., 2018). Few studies presented results regarding the time-lag response of NDVI to rainfall and PET. Additionally, the inclusion of PET was primarily reported in the studies using satellite imagery with low spatial resolution.

Spatial heterogeneity of semi-arid and arid vegetation and soil patterns at low resolution due to topographic, lithologic, hydrologic, and human disturbance variations is a source of confusion in the relationships between spectral indices and

climatic parameters. The use of Sentinel imagery with improved spatial resolution allows for better expression of vegetation versus bare soil and rocks distributions and thus may improve the sensitivity of NDVI to climatic parameters.

Thus, the aim of this study is to examine the relationships between NDVI extracted from Sentinel2 images with spatial resolution of 10 m/pixel and climatic parameters (rainfall and PET) at accumulation interval of 1 to 6 months for three years representing low (2017), average (2018) and high (2016) rainfall across the semi-arid to arid climatic gradient in Central Israel.

2. STUDY AREA

The study was conducted in Central Israel, which is located in the Eastern Mediterranean along a climatic gradient between Beit Guvrin in the Judean Lowland in the north, where the climate is semi-arid, with a mean annual temperature of 19.8 °C and 450 mm mean annual rainfall and Beer Sheva at the northern margins of the Negev Desert in the south, with a mean annual temperature of 21 °C and 200 mm annual rainfall (Figure 1a). Natural ecosystems along this transect change from dense Mediterranean shrublands with *Quercus calliprinos*, *Pistacia lentiscus*, *Ceratonia siliqua*, and *Rhamnus palaestinus* as dominant species, to open shrublands with the same species mixed with dwarf shrubs (primarily with *Sarcopoterium spinosum*) and herbaceous growth (e.g., Naveh, 1967, Danin and Orshan, 1990) to desert fringe Beta mainly composed of *Sarcopoterium spinosum* and *Thymelaea hirsuta* (Sternberg and Shoshany, 2001), and arid ecosystems characterized by moderate and low cover of *Sarcopoterium spinosum* with *Phlomis brachyodon*, *Echinops polyceras*,

*Corresponding author: sofiam@campus.technion.ac.il

Artemisia sieberi, *Thymelaea hirsute* and *Noaea mucronate* (e.g., Reisman-Berman et al., 2004).

Human disturbance caused by grazing, woodcutting, fires, and urbanization highly impact vegetation cover, life-forms composition, productivity, and biodiversity in this region. In addition, there are large areas afforested by the Israel Forest Service of the Jewish National Fund (JNF), mainly with *Pinus halepensis* plantations. Similar vegetation communities characterized by high spatial heterogeneity and patchiness of vegetation, soil and rocks are found in many other semi-arid Mediterranean regions (e.g., Naveh, 1967).

Following the experience gathered during a field study of plants' biomass (Sternberg and Shoshany, 2001) and remote sensing studies of soil (e.g., Svoray and Shoshany, 2004) and vegetation conditions (Shoshany and Svoray, 2002) and their joint patterns (Shoshany and Kelman, 2006; Roitberg and Shoshany, 2017) representative research sites were selected along the climatic transect. Utilizing air photographs and Google Earth high resolution (~2 meters) images we identified 38 plot areas of the size of 100x100 meters (Figure 1b) representing the less disturbed areas.

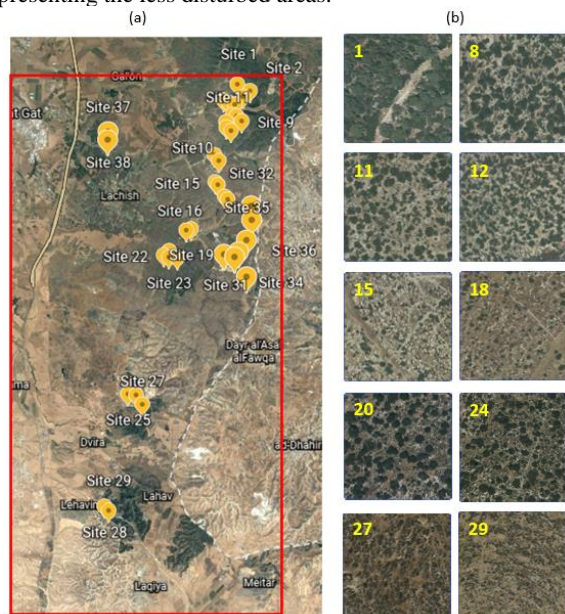


Figure 1: (a) Study area (adopted from Google Earth). (b) Examples of the research sites (adopted from <https://www.govmap.gov.il/>)

3. METHODS

The general methodology of the study is presented in Figure 2. The methodology starts with NDVI and climatic data preparation, continues with assessment of relationships between NDVI and rainfall and PET at different accumulation intervals for 38 sites across the climatic gradient zone, calculating per-pixel regression coefficients representing those relationships for Sentinel2 images between 2016 and 2018, and finally compare between SVM classification of multi-temporal NDVI and of regression coefficients.

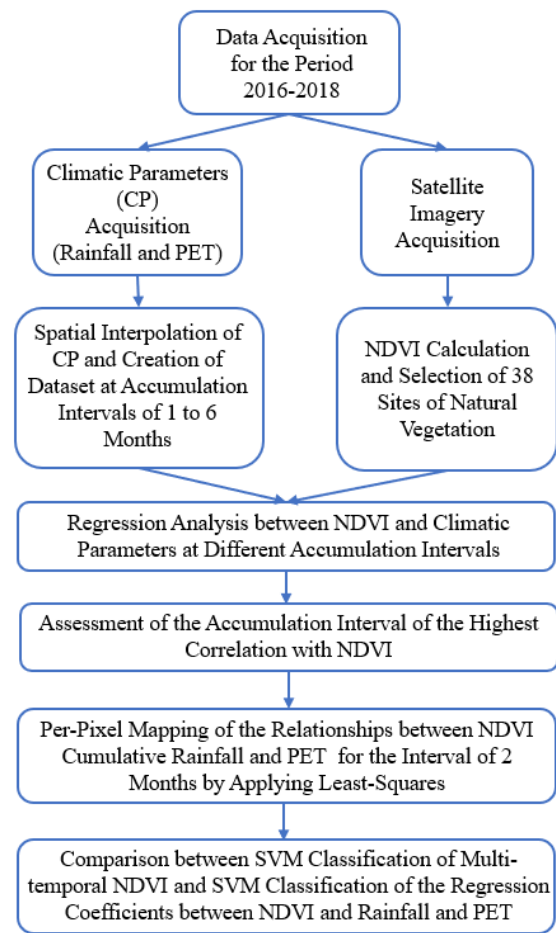


Figure 2: Flowchart of the study methodology.

3.1 Regression Analysis between NDVI and Climatic Parameters

The relationships between NDVI and climatic parameters (CP) (i.e., rainfall and PET accumulated for 1 to 6 months) were assessed along three years representing high (2016), low (2017), and average (2018) annual rainfall level.

Continuous maps of CPs were created from point data measured at sparsely located meteorological stations around the study area. For that purpose, several interpolation methods were compared based on cross-validation and tested on a synthetic dataset, representing the “truth” distribution of the mapped parameter. Following the results of cross-validation and synthetic data testing, the point monthly CPs were interpolated using Local Polynomials (LP) interpolation.

NDVI was calculated for 38 sites (100x100 meters each) (Figure 1b) across the study area from 25 Sentinel2 images captured during 2016, 2017 and 2018. Linear regressions were then fitted between NDVI and cumulative rainfall (Equation(1)) and PET (Equation(2)), accumulated for 1 to 6 months, for each research site of 38 sites of natural vegetation. Consequently, there is a defined linear regression for each site and accumulation interval. Relationships between NDVI and cumulative PET were previously assessed to be non-linear with the best linear fit on logarithmic scale for PET axis.

$$NDVI_i^s = a_{i,j}^s \times CR_{i,j}^s + b_{i,j}^s \quad (1)$$

$$NDVI_i^s = c_{i,j}^s \times \ln(CPET_{i,j}^s) + d_{i,j}^s \quad (2)$$

where NDVI is the index value for month i and research site s , s varying from 1 to 38; CR and $CPET$ are cumulative rainfall and PET respectively, calculated for month i , number of cumulative months j , varying from 1 to 6, and research site s ; a and b , c and d are slopes and intercepts of the regressions based on cumulative rainfall and PET respectively, calculated for month i , number of cumulative months j , and site s .

The level of correspondence between NDVI and rainfall and PET at different accumulation intervals was assessed by calculating determination coefficients for each research site and accumulation interval (R^2) and then generalizing the overall correlation per accumulation interval by averaging the determination coefficients.

3.2 Mapping of the Relationships between NDVI and Climatic Parameters

Further, the analysis of the relationships between NDVI and climatic parameters was extended from 38 sites to the whole study area by calculating linear regression coefficients between NDVI and CPs accumulated over the interval with the highest correlation to NDVI for each pixel in the Sentinel2 imagery using least squares technique. Two separate models were created, the first model based on the relationships between NDVI and rainfall (Equation(3)), and the second – on the relationships between NDVI and PET (Equation(4)).

$$NDVI_{p,m} = a_p \times CR_{p,m} + b_p \quad (3)$$

$$NDVI_{p,m} = c_p \times \ln(CPET_{p,m}) + d_p \quad (4)$$

where NDVI represents the values of the index calculated for pixel p on a month m ; CR and $CPET$ are cumulative rainfall and cumulative PET respectively, accumulated over the number of months, leading to the highest correlation, calculated for pixel p on a month m ; a and b are the slope and the intercept, respectively, of the rainfall-based model calculated for pixel p ; and c and d are the slope and the intercept, respectively, of the PET-based model calculated for pixel p . The slope and the intercept values of both models represent relationships between NDVI and studied climatic parameters and can be calculated for each pixel p using least-squares technique. The following equations ((5) and (6)) present the generalized matrix form of the linear regression equations ((3) and (4)) describing the relationships between NDVI and climatic parameters.

$$L_{p,25 \times 1} = A_{p,25 \times 2} \cdot x_{p,2 \times 1} \quad (5)$$

$$\begin{bmatrix} NDVI_{p,1} \\ NDVI_{p,2} \\ \vdots \\ NDVI_{p,24} \\ NDVI_{p,25} \end{bmatrix} = \begin{bmatrix} CP_{p,1} & 1 \\ CP_{p,2} & 1 \\ \vdots & 1 \\ CP_{p,24} & 1 \\ CP_{p,25} & 1 \end{bmatrix} \cdot \begin{bmatrix} slope_p \\ intercept_p \end{bmatrix} \quad (6)$$

where L_p is a vector of NDVI values calculated for each pixel p and 25 dates corresponding to the dates of Sentinel2 images, A_p is a matrix of partial derivatives of the unknown coefficients calculated for pixel p where CP_p is a climatic parameter (cumulative rainfall or cumulative PET) estimated for pixel p , x_p is a vector of unknown coefficients (a_p, b_p) and (c_p, d_p)

for the rainfall-based model and the PET-based model, respectively. Thus, the unknown coefficients for pixel p , which are the slope and the intercept of the linear models representing the relationships between NDVI and climatic parameters, can be calculated by the following equation (7):

$$x_p = (A_p^T A_p)^{-1} \cdot A_p^T L_p \quad (7)$$

Afterwards, the calculated per-pixel coefficients of the relationships between NDVI and cumulative rainfall and PET were stacked into a 4-layer image, where each layer represents a single coefficient.

Next, SVM supervised classification was implemented once on the image representing the distribution of the regression coefficients and then on a multi-temporal image, combining 25 layers of NDVI corresponding to the dates of the Sentinel2 images utilized in the study. SVM classification was used to classify the two types of data into 9 classes, while training and validation areas were carefully selected using air photographs with spatial resolution of 20 cm/pixel (<https://www.govmap.gov.il>). Accuracies of both classifications were assessed by confusion matrices.

4. RESULTS AND DISCUSSION

4.1 Regression Analysis between NDVI and Climatic Parameters

The results of the determination coefficients (R^2) of the linear regression analysis between NDVI and rainfall and PET at accumulation intervals of 1 to 6 months (statistically significant) calculated per each of the 38 research sites and their average value for all the research sites in the last row are presented in Table 1 and Table 2. The results suggest that the highest correlation between NDVI and studied climatic parameters, is obtained for the accumulation interval of two months for both, rainfall and PET. This finding is consistent with the results of previous studies (e.g., Nicholson et al., 1990; Nicholson and Farrar, 1994; Chamaille-Jammes et al., 2006; Vicente-Serrano et al., 2013; Chen et al., 2014; Dagnachew et al., 2020), which conclude that vegetation indices have lower correlation with climatic parameters accumulated for more than 3 months.

The slope and intercept coefficients of the linear regressions calculated between NDVI and climatic parameters at accumulation interval of 2 months present the spectral reflectance response to changes in climatic and habitat conditions along the studied climatic gradient. The slope and intercept coefficients are expected to assist in mapping of vegetation conditions along the semi-arid to arid climatic transect.

4.2 Mapping of the Relationships between NDVI and Climatic Parameters

The linear regression coefficient layers and the multi-temporal NDVI layers were classified into 9 classes (Figure 3) using SVM supervised classification. Table 3 presents the description of the classes.

Figure 4 presents the results of SVM multi-temporal classification of the 25 layers of NDVI corresponding to the dates of Sentinel2 images (Figure 4a) and the results of SVM classification of the extended regression analysis between NDVI and rainfall and PET accumulated for 2 months (Figure 4b).

Area	R-Squared of NDVI-Rainfall Regressions					
	Cumulative Months					
	1	2	3	4	5	6
1	0.59	0.70	0.71	0.49	0.30	0.20
2	0.57	0.67	0.69	0.48	0.30	0.21
3	0.48	0.69	0.83	0.64	0.47	0.36
4	0.67	0.86	0.78	0.51	0.29	0.19
5	0.64	0.84	0.81	0.55	0.33	0.22
6	0.64	0.86	0.80	0.53	0.32	0.22
7	0.68	0.80	0.71	0.46	0.25	0.16
8	0.69	0.79	0.68	0.41	0.22	0.14
9	0.67	0.80	0.70	0.43	0.24	0.15
10	0.60	0.81	0.81	0.58	0.38	0.27
11	0.66	0.82	0.77	0.52	0.31	0.20
12	0.51	0.69	0.79	0.63	0.45	0.35
13	0.62	0.86	0.80	0.55	0.35	0.25
14	0.61	0.86	0.80	0.54	0.33	0.22
15	0.69	0.89	0.80	0.52	0.31	0.21
16	0.66	0.84	0.82	0.57	0.36	0.26
17	0.65	0.91	0.81	0.52	0.31	0.21
18	0.64	0.85	0.77	0.48	0.28	0.18
19	0.68	0.82	0.68	0.40	0.21	0.12
20	0.67	0.83	0.73	0.45	0.26	0.17
21	0.72	0.89	0.77	0.49	0.30	0.20
22	0.67	0.86	0.76	0.50	0.30	0.20
23	0.71	0.86	0.72	0.46	0.27	0.18
24	0.65	0.86	0.79	0.53	0.33	0.23
25	0.67	0.89	0.77	0.48	0.28	0.18
26	0.68	0.89	0.75	0.46	0.26	0.16
27	0.67	0.87	0.73	0.44	0.25	0.16
28	0.66	0.87	0.76	0.49	0.31	0.19
29	0.65	0.87	0.75	0.47	0.28	0.17
30	0.70	0.84	0.71	0.43	0.24	0.15
31	0.66	0.85	0.71	0.43	0.24	0.15
32	0.56	0.81	0.75	0.48	0.28	0.19
33	0.64	0.86	0.74	0.46	0.26	0.17
34	0.63	0.86	0.75	0.48	0.29	0.19
35	0.69	0.86	0.75	0.47	0.28	0.18
36	0.65	0.86	0.74	0.46	0.26	0.16
37	0.60	0.83	0.83	0.57	0.35	0.24
38	0.64	0.85	0.78	0.51	0.29	0.19
Mean	0.64	0.83	0.76	0.50	0.30	0.20

Table 1: Determination coefficients of the linear regression analysis between NDVI and rainfall accumulated for 1 to 6 months.

Area	R-Squared of NDVI-PET Regressions					
	Cumulative Months					
	1	2	3	4	5	6
1	0.75	0.75	0.61	0.38	0.18	0.06
2	0.72	0.72	0.59	0.37	0.18	0.06
3	0.61	0.71	0.67	0.50	0.31	0.16
4	0.84	0.86	0.68	0.40	0.18	0.05
5	0.82	0.86	0.70	0.44	0.21	0.07
6	0.81	0.86	0.71	0.44	0.21	0.07
7	0.84	0.81	0.62	0.36	0.15	0.04
8	0.83	0.78	0.57	0.31	0.12	0.02
9	0.82	0.79	0.59	0.33	0.14	0.03

10	0.79	0.85	0.73	0.49	0.26	0.10
11	0.82	0.83	0.66	0.40	0.19	0.06
12	0.68	0.77	0.70	0.52	0.32	0.16
13	0.77	0.82	0.68	0.44	0.22	0.08
14	0.72	0.77	0.64	0.41	0.19	0.06
15	0.79	0.83	0.67	0.41	0.18	0.05
16	0.78	0.82	0.68	0.43	0.22	0.08
17	0.75	0.81	0.66	0.41	0.19	0.05
18	0.79	0.82	0.66	0.40	0.18	0.05
19	0.83	0.81	0.60	0.33	0.12	0.02
20	0.80	0.80	0.61	0.35	0.14	0.03
21	0.80	0.83	0.65	0.38	0.17	0.04
22	0.79	0.81	0.64	0.38	0.17	0.05
23	0.80	0.80	0.61	0.35	0.15	0.04
24	0.77	0.81	0.66	0.41	0.20	0.06
25	0.80	0.84	0.68	0.41	0.18	0.05
26	0.80	0.83	0.65	0.38	0.16	0.04
27	0.81	0.82	0.64	0.37	0.16	0.04
28	0.75	0.78	0.63	0.39	0.18	0.06
29	0.77	0.80	0.65	0.39	0.18	0.05
30	0.78	0.78	0.60	0.34	0.13	0.02
31	0.75	0.76	0.59	0.34	0.14	0.03
32	0.74	0.80	0.67	0.43	0.21	0.07
33	0.78	0.81	0.65	0.39	0.17	0.04
34	0.74	0.79	0.64	0.39	0.17	0.05
35	0.80	0.82	0.65	0.38	0.17	0.04
36	0.78	0.81	0.65	0.38	0.16	0.04
37	0.80	0.82	0.67	0.43	0.21	0.07
38	0.82	0.81	0.63	0.37	0.16	0.04
Mean	0.78	0.81	0.65	0.40	0.18	0.06

Table 2: Determination coefficients of the linear regression analysis between NDVI and PET accumulated for 1 to 6 months.



Figure 3: Land-cover classes for SVM classification.

Herb.	Herbaceous vegetation
B. Areas	Buildings, quarry, military complex
Asphalt	Asphalt (highways)
Forest	Planted Pine Forest
D. Veg.	Dense Vegetation
M. Veg.	Medium Vegetation
S. Veg.	Sparse Vegetation
Batha	Dwarf Shrubs
Fire Areas	Areas that were set on controlled fires by the military

Table 3: Description of the land-cover classes.

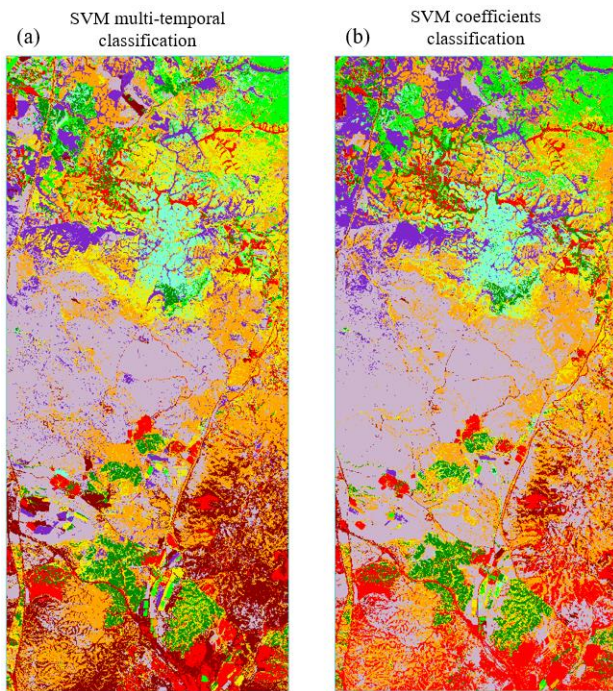


Figure 4: Results of SVM supervised classification: (a) SVM multi-temporal classification; (b) SVM classification of linear regression coefficients.

Accuracy assessment of both classifications was performed by creating confusion matrices using ground truth data, carefully selected for validation for the land-cover classes listed in Figure 3. Table 4 and Table 5 present a confusion matrix and accuracy measures for SVM multi-temporal classification and SVM coefficients classification respectively. According to the overall accuracy and Kappa coefficient measures, the SVM multi-temporal classification (overall accuracy of 91.35%, Kappa coefficient of 0.9007) slightly outperforms the SVM coefficients classification (overall accuracy of 84.21%, Kappa coefficient of 0.8186). The values of Kappa coefficients indicate that both, SVM multi-temporal classification (Kappa coefficient of 0.9007) and SVM coefficients classification (Kappa coefficient of 0.8186), are in good agreement with the ground truth.

SVM coefficients classification's confusion matrix (Table 5) shows that most of the inaccuracies come from the confusion between the classes representing forest and dense vegetation (omission error of 34.87% for the forest class), between the classes representing sparse vegetation and batha (omission error of 30.04% for the sparse vegetation class), and between the classes representing asphalt and built areas (omission error of 66.51% for the asphalt class).

Confusion between forest and dense vegetation classes in the SVM coefficients classification can be explained by similar water-use regime of these types of vegetation. Confusion between sparse vegetation and batha can also be explained by similar water-use regime, as well as by mixture of the two classes in some areas.

Confusion between built areas and asphalt can be explained by the following instances: (1) there are asphalt areas inside built areas, and (2) similar relationships with climatic parameters, hence similar regression coefficients.

		Ground Truth									
class		herb. veg.	forest	built areas	dense veg.	medium veg.	sparse veg.	batha	asphalt	fire areas	total
Classification	herb. veg.	96.99	0	0	0	0	0.06	0.06	0.2	2.48	5.12
	forest	0	84.64	0	2.29	0.13	0.36	0	0.07	0	16.46
	built areas	0	0	97.8	0	0	0	0	31.83	0	13.7
	dense veg.	0	10	0	93.98	5.9	0.89	0.39	0	0	16.45
	medium veg.	1.3	5.11	0	3.45	92.6	1.82	0.2	0	0	10.26
	sparse veg.	1.12	0.09	0.07	0.28	1.12	90.16	0.25	1.26	0	9.22
	batha	0.59	0.15	0.09	0	0.26	6.71	99.06	7.29	1.18	16.09
	asphalt	0	0	2.01	0	0	0	0.02	58.36	3.99	3.25
	fire areas	0	0	0.02	0	0	0	0.02	0.99	92.34	9.45
	total	100	100	100	100	100	100	100	100	100	100
Overall Accuracy		% 91.35%									
Kappa Coefficient		0.9007									

Table 4: Confusion matrix and accuracy measures of SVM multi-temporal classification.

		Ground Truth									
class		herb. veg.	forest	built areas	dense veg.	medium veg.	sparse veg.	batha	asphalt	fire areas	total
Classification	herb. veg.	97.11	0	0	0	0	0.36	1.39	0	0	5.09
	forest	0	65.13	0.02	1.66	4.65	0.06	0	0.27	0	13.05
	built areas	0	0	94.64	0	0	0	0.72	54.84	0	14.44
	dense veg.	0	26.21	0	97.95	2.79	2.86	1.66	0.07	0	20.21
	medium veg.	2.53	8.34	0	0.06	90.48	4.44	0.45	0	0	10.53
	sparse veg.	0.18	0.33	0	0.1	1.95	69.96	1.84	1.19	0	7.5
	batha	0.18	0	3.37	0.24	0.13	22.32	93.74	6.37	3.09	17.37
	asphalt	0	0	1.54	0	0	0	0	33.49	0.03	1.68
	fire areas	0	0	0.42	0	0	0	0.2	3.78	96.88	10.12
	total	100	100	100	100	100	100	100	100	100	100
Overall Accuracy		% 84.21%									
Kappa Coefficient		0.8186									

Table 5: Confusion matrix and accuracy measures of SVM coefficients classification.

Although SVM coefficients classification is less accurate, it incorporates climatic information beside spectral data, integrating water-use regime influence on land-cover, while SVM multi-temporal classification consists entirely of the spectral data, therefore we can assume that they contain different information. Comparative analysis of information content indicated that SVM multi-temporal classification mostly produced much more homogeneous and generalized patterns of the landscape units, even in cases, where the surface represented a mixture of several surface cover types. While SVM coefficients classification provided higher spatial sensitivity to the variation of these cover types across the climatic gradient.

5. CONCLUSIONS

The aim of this study was to examine and map the relationships between NDVI and climatic parameters (rainfall and PET) over desert fringe ecosystems of high geodiversity of vegetation and soil patterns. The results of the regression analysis reveal that variations in NDVI over the studied period are best described by the locally fitted linear regression between the index and rainfall and PET accumulated for two months. Since the slope and intercept coefficients can be perceived as representing the water use regime at each pixel, the broad similarity between the classification results suggests that multi-temporal NDVI typologies correspond water use regime typologies across desert fringe ecosystems at the margins of Mediterranean regions.

ACKNOWLEDGEMENTS

The Israeli Space Agency, Ministry of Science Research Program (#3-14722), the Technion Asher Space Research Grant Scheme and the Technion Graduate students' Scholarship program are most appreciated for their support of Mrs. Mozhaeva PhD research.

REFERENCES

- Al-Bakri, J. T., Suleiman, A. S., 2004, NDVI response to rainfall in different ecological zones in Jordan. *International Journal of Remote Sensing*, 25:19, 3897-3912.
- Chamaille-Jammes, S., Fritz, H., 2009, Precipitation-NDVI relationships in eastern and southern African savannas vary along a precipitation gradient. *International Journal of Remote Sensing*, 30:13, 3409-3422.
- Chamaille-Jammes, S., Fritz, H., Murindagomo, F., 2006, Spatial patterns of the NDVI-rainfall relationship at the seasonal and interannual time scales in an African savanna. *International Journal of Remote Sensing*, 27:23, 5185-5200.
- Chen, T., de Jeu, R. A. M., Liu, Y. Y., van der Werf, G. R., Dolman, A. J., 2014, Using satellite-based soil moisture to quantify the water driven variability in NDVI: A case study over mainland Australia. *Remote Sensing of Environment*, 140, 330-338.
- Dagnachew, M., Kebede, A., Moges, A., Abebe, A., 2020, Effects of climate variability on Normalized Difference Vegetation Index (NDVI) in the Gojeb River Catchment, Omo-Gibe Basin, Ethiopia. *Advances in Meteorology*, ID 8263246.
- Danin, A., Orshan, G., 1990, The distribution of Raunkiaer life forms in Israel in relation to the environment. *Journal of Vegetation Science*, 1:1, 41-48.
- Dorman, M., Svoray, T., Perevolotsky, A., Sarris, D., 2013, Forest performance during two consecutive drought periods: Diverging long-term trends and short-term responses along a climatic gradient. *Forest Ecology and Management*, 310, 1-9.
- Gordo, O., Sanz, J.J., 2010, Impact of climate change on plant phenology in Mediterranean ecosystems. *Global Change Biology*, 16(3), 1082-1106.
- Gouveia, C.M., Trigo, R.M., Begueria, S., Vicente-Serrano, S. M., 2017, Drought impacts on vegetation activity in the Mediterranean region: An assessment using remote sensing and multi-scale drought indicators. *Global and Planetary Change*, 151, 15-27.
- Islam, M., Mamun, M. I., 2015, Variations of NDVI and its association with rainfall and evapotranspiration over Bangladesh. *Rajshahi University Journal of Science and Engineering*, 43, 21-28.
- Lamchin, M., Lee, W.-K., Jeon, S.W., Wang, S.W., Lim, C.H., Song, C., Sung, M., 2018, Long-term trend and correlation between vegetation greenness and climate variables in Asia based on satellite data. *Science of the Total Environment*, 618, 1089-1095.
- Malhi, Y., Franklin, J., Seddon, N., Solan, M., Turner, M.G., Field, C.B., Knowlton, N., 2020, Climate change and ecosystems: Threats, opportunities and solutions. *Philosophical Transactions of the Royal Society B*, 375(1794), 20190104.
- Munson, S. M., Long, A. L., Wallace, C. S. A., Webb, R. H., 2016, Cumulative drought and land-use impacts on perennial vegetation across a North American dryland region. *Applied Vegetation Science*, 19, 430-441.
- Naveh, Z., 1967, Mediterranean ecosystems and vegetation types in California and Israel. *Ecology*, 48:3, 445-459.
- Nicholson, S. E., Davenport, M. L., Malo, A. R., 1990, A comparison of the vegetation response to rainfall in the Sahel and East Africa, using Normalized Difference Vegetation Index from NOAA AVHRR. *Climatic Change*, 17, 209-241.
- Nicholson, S. E., Farrar, T. J., 1994, The influence of soil type on the relationships between NDVI, rainfall and soil moisture in semiarid Botswana. I. NDVI response to rainfall. *Remote Sensing of Environment*, 50, 107-120.
- Reisman-Berman, O., 2004, *Mechanisms controlling spatiotemporal patterns of shrubland patchiness: the case study of *Sarcopoterium spinosum* (L) Spach* (Doctoral dissertation, Ph. D. Thesis. Ben-Gurion University of the Negev).
- Roitberg, E., Shoshany, M., 2017, Can spatial patterns along climatic gradients predict ecosystem responses to climate change? Experimenting with reaction-diffusion simulations. *PLoS ONE*, 14(4): e0174942.
- Shoshany, M., Kelman, E., 2006, Assessing mutuality of change in soil and vegetation patch pattern characteristics by means of Cellular Automata simulation. *Geomorphology*, 77(1-2), 35-46.
- Shoshany, M., Kutiel, P., Lavee, H., 1996, Monitoring temporal vegetation cover changes in Mediterranean and arid ecosystem using a remote sensing technique: case study of the Judean Mountain and the Judean Desert. *Journal of Arid Environment*, 32, 1-13.
- Shoshany, M., and Karnibad, L., 2011, Mapping Shrubland Biomass Along Mediterranean Climatic Gradients: the synergy of Rainfall and NDVI-Based Models. *International Journal of Remote Sensing*, 32(24), 9497-9508.
- Shoshany, M., and Karnibad, L., 2015, Relative Water Use Efficiency and Shrublands Biomass along a Semi-Arid Climatic Gradient: A Remote Sensing Study. *Remote Sensing (Online)*7, 2283-2301.
- Shoshany, M., Svoray, T., 2002, Multidate Adaptive Unmixing and its Application to Analysis of Ecosystem Transitions along a Climatic Gradient. *Remote Sensing of Environment*, 82, 5-20.
- Sternberg, M., Shoshany, M., 2001, Aboveground biomass allocation and water content relationships in Mediterranean trees and shrubs in two climatological regions in Israel. *Plant Ecology*, 157(2), 173-181.
- Svoray, T., Shoshany, M., 2004, Multi-scale analysis of intrinsic soil factors from SAR-based mapping of drying rates. *Remote sensing of environment*, 92(2), 233-246.
- Vicente-Serrano, S. M., Gouveia, C., Camarero, J. J., Begueria, S., Trigo, R., Lopez-Moreno, J. I., Azorin-Molina, C., Pasho, E., Lorenzo-Lacruz, J., Revuelto, J., Moran-Tejeda, E., Sanchez-Lorenzo, A., 2013, Response of vegetation to drought time-scales across global land biomes. *Proceedings of the National Academy of Sciences of the United States of America*, 110(1), 52-57.